



Sandwich-structured Ag/graphene/Au hybrid for surface-enhanced Raman scattering



Aiping Liu ^{a,b,*}, Tao Xu ^a, Jian Tang ^a, Huaping Wu ^c, Tingyu Zhao ^a, Weihua Tang ^d

^a Center for Optoelectronics Materials and Devices, Zhejiang Sci-Tech University, Hangzhou 310018, China

^b State Key Lab of Silicon Materials, Zhejiang University, Hangzhou 310027, China

^c Key Laboratory of E&M (Zhejiang University of Technology), Ministry of Education & Zhejiang Province, Hangzhou 310032, China

^d State Key Laboratory of Information Photonics and Optical Communication, Beijing University Posts and Telecommunications, Beijing 100876, China

ARTICLE INFO

Article history:

Received 8 November 2013

Received in revised form 5 December 2013

Accepted 6 December 2013

Available online 18 December 2013

Keywords:

Metallic plasmons

Reduced graphene oxide

Sandwich structure

Surface-enhanced Raman scattering

Electrochemical deposition

ABSTRACT

The Ag/graphene/Au nanostructure as an efficient surface enhanced Raman scattering (SERS)-active substrate was fabricated by sandwiching the reduced graphene oxide (rGO) between plasmonic silver dendrites and gold nanoparticles layers by a simple electrodeposition method. The surface plasmons aroused in the Ag-rGO interface could be effectively transferred from the silver to the top gold by rGO interlayer, which favored the higher SERS activity of Ag/rGO/Au hybrid compared to the Ag/rGO and Au/rGO/Au ones due to the more localized plasmon resonance on the gold surface. Furthermore, the reduction degree of rGO interlayer impacted the nucleation and growth of gold on the rGO surface and therefore the Raman signal for Rhodamine B molecules absorbed on the Ag/rGO/Au sandwich nanostructure. The rGO sheets and the top gold nanoparticles film also effectively protected the silver dendrites from oxidation under ambient condition. This Ag/rGO/Au sandwich nanostructure was useful for the development of an efficient SERS-based chemical sensor because of the simply fabrication, adjustable SERS activity, long-term stability and high reproducibility.

© 2013 Elsevier Ltd. All rights reserved.

1. Introduction

Surface-enhanced Raman scattering (SERS) that was discovered in 1974 [1] has attracted increasing attention as a powerful analytical technique in chemical and biological detections for low-concentration molecules, DNA, pathogens, etc [2–4]. Plasmonic silver or gold nanostructures with different morphologies are usually selected as the SERS-active substrates [5,6]. Silver has a greater enhancement factor compared to gold; however, its bad chemical stability and biocompatibility hinder its long-term use, especially for biomolecule detection [7]. Recent research indicates that coating silver nanoparticles (NPs) with stable materials such as ultrathin diamond-like carbon (DLC) [8], silica [9], titania [10] and graphene oxide (GO) [11] can effectively protect them from being oxidized. For example, Liu et al. fabricated a novel SERS-active substrate with prominent enhancement of Raman signals and excellent chemical stability by coating ultrathin DLC film on the surface of plasmonic silver NPs [8]. Furthermore, the gold NPs film with excellent chemical stability and biocompatibility can compensate the weaknesses of silver, and various Ag-Au hybrid systems have been

designed to enhance the Raman signal of adsorbed molecules on the active substrates [12–14]. The gold monolayer deposited on the silver dendrites provided a suitable route for long-term employment of silver-based SERS substrate [12]. The gold shell on the silver NPs (Ag@Au) could effectively improve the biocompatibility and stability of silver [13] though the considerable difficulty in accurately controlling reaction conditions to obtain well-defined shell thickness with high reproducibility and effectively separating Ag@Au NPs from heterogeneous impurities before use.

Additionally, a sandwich-structured composite, which is composed of plasmonic metal and dielectric or semiconductor layer, has the potential advantage as SERS-active substrate [9,15–17] by combining the characters of metallic plasmons and stable interlayer. For example, Feng et al. constructed Ag/SiO₂/Au sandwich configuration by using dielectric SiO₂ as an interlayer, and this three-layer composite showed improved SERS performance not only in Raman intensity but also in stability and reproducibility since the extra interfaces made the plasmons transfer more efficiently [9]. As a fine SERS-active material [18,19], the two-dimensional graphene (GE) or GO or reduced graphene oxide (rGO) nanosheet with carbon atoms packed in a hexagonal lattice was also used as the interlayer to construct metal/GE/metal three-layer structure [20,21]. For example, Zhang et al. prepared Au@Ag/GO/Au@Ag sandwich nanostructure and confirmed the enhanced SERS signal due to the

* Corresponding author. Tel.: +86 571 86843468; fax: +86 571 86843468.

E-mail address: liuap1979@gmail.com (A. Liu).

plenty of hot spots on their surfaces and the unique structure of GO sheets [20]. We also succeeded in developing an Au/rGO/Au sandwich structure with SERS activity [21]. Since the chemical enhancement nature of rGO, this sandwich structure with rGO interlayer is useful for understanding the coexistence of the electromagnetic mechanism and chemical mechanism among the metal nanostructures, GE (or rGO) and the adsorbed analyte. The oxygen functionalities at the GE surface play an important role in nucleation and growth of metal nanostructures and provide the opportunity to create more “hot spots” between metal NPs [22]. The distribution of metal NPs on the surface of GE sheets can be easily controlled by the functionalities of GE sheets [21,22]. This is a unique advantage of GE sheets compared to dielectric interlayer. Therefore, the resulted Ag/rGO/Au sandwich structure with adjustable plasmon structure and efficient plasmon transfer between extra interfaces might present more excellent SERS activity compared to the Au/rGO/Au one. In this paper, we embedded the rGO sheets between the branched silver and hemispherical gold nanostructures to build the Ag/rGO/Au sandwich configuration on the nitrogen doped DLC (DLC:N) film by a convenient and low-cost electrodeposition method. Plasmonic gold nanostructures were regulated by changing the reduction degree of rGO sheets. The obtained Ag/rGO/Au hybrid exhibited a strong SERS signal for low-concentration Rhodamine B (RhB) molecules due to the coupling of metallic plasmons and rGO sheets and good stability and reproducibility due to the protection of rGO and gold NPs layers for silver dendrites.

2. Experimental

2.1. Reagents and materials

Graphite (50 μm) was purchased from Shanghai Carbon Co., Ltd. HAuCl₄·3H₂O (purity 99.99%), AgNO₃ (purity 99.99%) and RhB (purity 98%) were supplied by Sigma, USA. All other chemicals were of analytical grade and used without further purification. The water was obtained from a Millipore Q purification system (resistivity > 18 M Ω cm).

2.2. Preparation of Ag/rGO/Au sandwich configuration

The 100-nm-thick DLC:N films (4.0 at.% N) were deposited on silicon substrates by a filtered cathodic vacuum arc system as described in literature [23]. The electrochemical experiments were performed in a three-electrode system at room temperature by an electrochemical workstation (CHI630D, Shanghai Huachen) with a Si/DLC:N sheet, a platinum foil and a saturated calomel electrode (SCE) as the working, counter and reference electrodes, respectively. The solutions in all electrochemical experiments were nitrogen-saturated. The Si/DLC:N specimens were first immersed into a 75 mM KNO₃ solution containing 3 mM AgNO₃ to electrodeposit silver dendrites on the DLC:N surfaces at -0.3 V (vs. SCE) for 1200s. Then a 0.5 mg/mL exfoliated GO aqueous solution prepared by modified Hummers method [24,25] was spin-coated on the Si/DLC:N/Ag surfaces at 1500 rpm for 30s. The GO layers were further electrochemically reduced in a 20 mM KH₂PO₄ supporting electrolyte with the potential controlled from 0 V to -2 V (vs. SCE) at 0.05 V/s. The reduction degree of GO were easily controlled by changing the reduction time (from 0s to 800s). Subsequently, the electrodeposition of gold NPs on Ag/GO, Ag/rGO and silver dendrites was carried out at -0.8 V (vs. SCE) for 400s in a 75 mM KH₂PO₄ solution containing 2 mM HAuCl₄ [21], and the specimens were correspondingly labeled as Ag/GO/Au, Ag/rGO/Au and Ag/Au, respectively. The Au/rGO/Au sandwich structure was also prepared as the reference.

2.3. Characterization

The morphologies of silver and gold nanostructures were observed by a scanning electron microscopy (SEM, Hitachi S4800). The elemental composition and core level spectra of hybrids were collected by the X-ray photoemission spectroscopy (XPS, KRATOS AXIS ULTRA-DLD) with the binding energies calibrated by C1s as reference energy. All samples for SERS measurement were incubated in the different concentrations of RhB aqueous solutions for 24 h to form an adsorbed monolayer and the SERS spectra were acquired with a Thermo Fisher DXR Raman spectrometer equipped with an objective (50 \times) using a He-Ne laser ($\lambda=632.8$ nm). The Raman signal intensity of RhB was normalized by using a silicon peak at ~ 1000 cm⁻¹ as the standard.

3. Results and discussion

3.1. Microstructures of Ag/rGO/Au sandwich configurations

Fig. 1(a) shows the morphology of dendritic silver nanostructure fabricated by the electrochemical deposition on the Si/DLC:N surface. The sizes of the main branches are in the range from 100 nm to 800 nm. The formation mechanism of silver dendrites might be attributed to the localized microscopic electrochemical cell model and diffusion-limited aggregation process of small particles or nanoclusters [26–28]. After the rGO deposition (the reduction time of 80s), the silver dendrites underneath the wrinkled and semi-transparent rGO sheets are still clearly distinguishable (Fig. 1b). However, the dendrites topology cannot be obtained when the silver was directly deposited on the rGO surface in the same deposition condition. This might be attributed to the carbon atoms with dangling bonds or oxygen functionalities as the defect sites on the rGO surface, which result in uniform nucleation and deposition of silver with an average size of 65 nm (Fig. 1c) [29]. After gold deposition on the rGO surface, the apparent three-layer structure is observed (Fig. 1d) and the densely-packed gold NPs with an average size about 15 nm are uniformly distributed on the rGO surface.

Furthermore, the oxygen functionalities on the rGO surface, which are related to the reduction degree of GO, affect the morphologies and quantities of metallic nanostructures on rGO sheets [21,22]. By changing the reduction time of GO, we obtain rGO sheets with different reduction degrees as shown in Fig. 2. The cyclic voltammograms of GO reduction on the Si/DLC:N/Ag surface indicate that the reduction starts from -0.90 V with a peak around -1.50 V due to the reduction of oxygen-containing groups on the GO (Fig. 2a). The current increase at the potential over -1.6 V is related to the hydrogen evolution. Furthermore, the current of reduction peak of GO decreases with a slight right shift as the potential cycling proceeds. When the reduction time increases to 800s, the reduction current peak reaches a minimum. This demonstrates that rGO sheets with different reduction degrees are easily obtained by the electrochemical method. The Raman spectra of rGO sheets with different reduction degrees (Fig. 2b) indicate that the intensity ratio of D peak (1336 cm⁻¹) to G peak (1594 cm⁻¹) (I_D/I_G) increases from 0.87 for GO to 1.46 for rGO with 400s reduction and to 1.72 for rGO with 800s reduction. This might be explained that the distortion of 6-fold rings caused by oxygen functionalities is removed after GO deoxidation [30], and the carbon lattice returns to an essentially graphitic state with highly defected, resulting in the increase of I_D/I_G ratio. The XPS results show that the C/O atomic percentage increases from 1.66 for GO to 3.37 for 400s-reduced rGO to 4.75 for 800s-reduced rGO, demonstrating enhanced reduction degree from GO to rGO [21]. Fig. 3 shows the SEM images of Ag/rGO/Au hybrids with different reduced rGO sheets. We observe an increase in gold

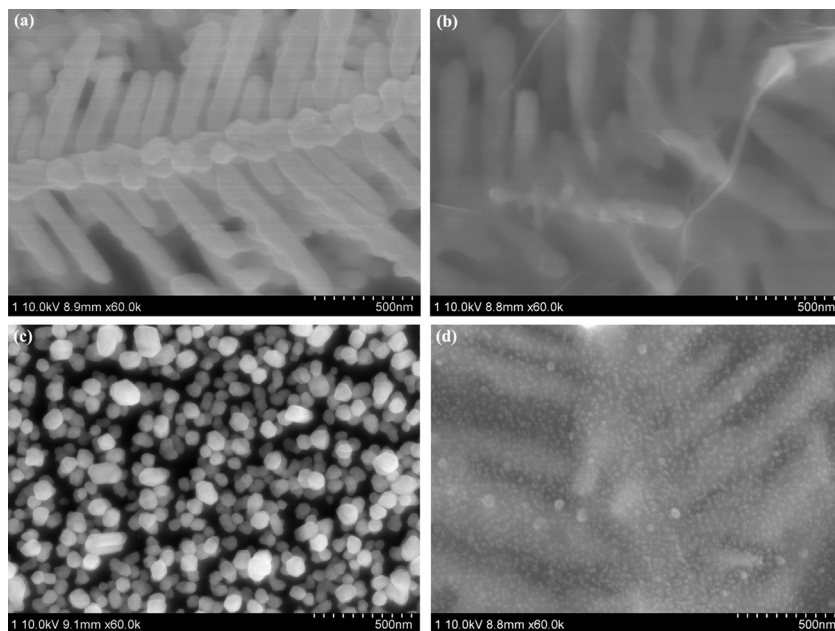


Fig. 1. Scanning electron microscopy images of (a) branched Ag, (b) Ag/rGO, (c) rGO/Ag and (d) Ag/rGO/Au sandwich structure on the Si/DLC:N substrates. The reduction time of GO was 80s.

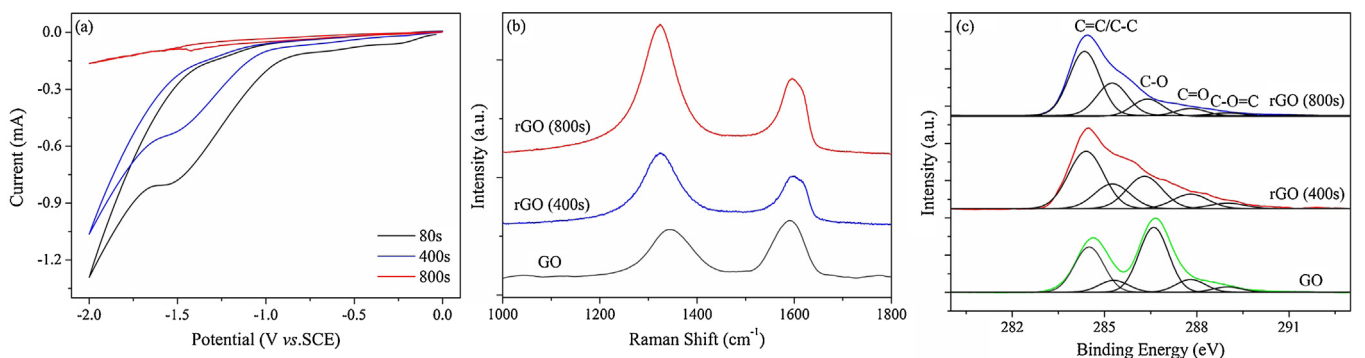


Fig. 2. (a) Cyclic voltammograms of GO electrochemical reduction on Si/DLC:N/Ag surfaces for different times. (b) Raman spectra and (c) C1s spectra of GO and rGO sheets with different reduction times.

particle size as well as the aggregation of particles with the increasing reduction degree of rGO. The gold NPs on GO surface have an average size of 14 nm (Fig. 3a) which increases to 23 nm and 34 nm when the rGO sheets are reduced by 400s (Fig. 3b) and 800s (Fig. 3c), respectively. This indicates that the oxygen-containing groups play an important role in gold nucleation and growth. Fewer oxygen functionalities on the rGO surface provide less reactive sites for gold nucleation, which makes gold seeds be more inclined to form larger particles. This is consistent with previous reports [21,22,31].

3.2. SERS responses of RhB molecules on Ag/rGO/Au sandwich structures

Fig. 4(a) shows the SERS responses of 10^{-6} M RhB adsorbed on different configurations. An evident Raman signal related to RhB can be detected on the silver dendrites deposited on the Si/DLC:N substrate due to the localized electromagnetic field enhancement created by surface plasmon polaritons at roughened surfaces and sharp edges of silver dendrites [12]. After the rGO sheets are coated

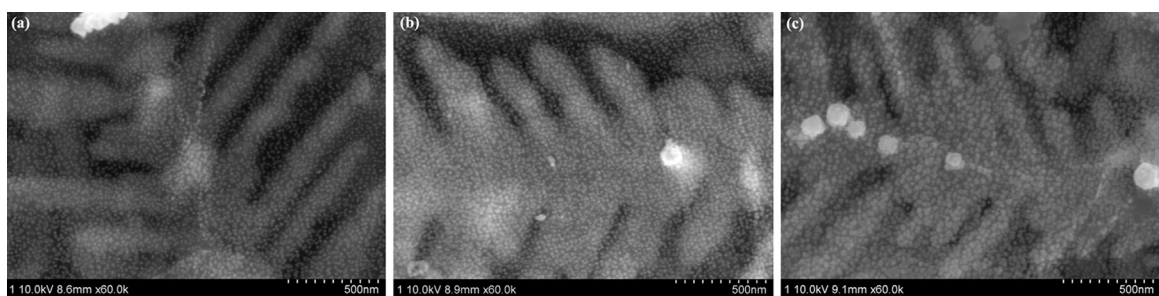


Fig. 3. Scanning electron microscopy images of (a) Ag/GO/Au, (b) and (c) Ag/rGO/Au sandwich structures with the reduction times of rGO sheets of (b) 400s and (c) 800s, respectively.

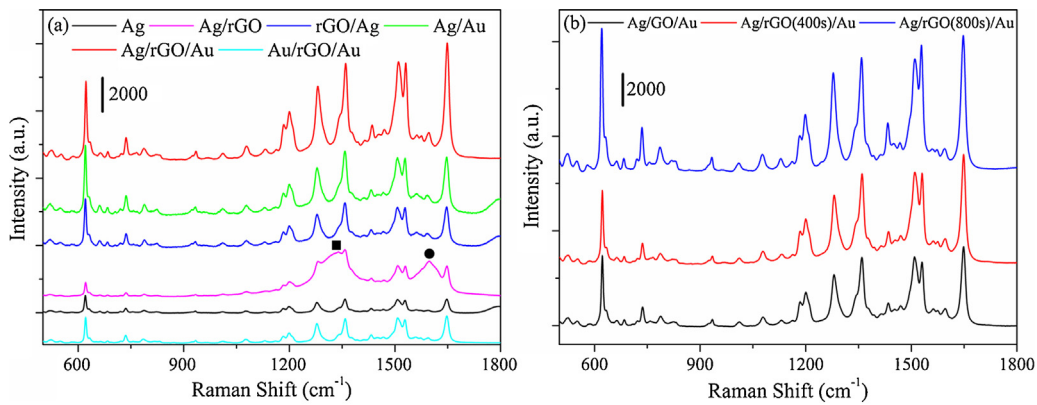


Fig. 4. SERS spectra of 10^{-6} M RhB adsorbed on (a) different substrates and (b) Ag/GO/Au and Ag/rGO/Au sandwich structures with different reduction degrees of rGO interlayers. The D peak and G peak of rGO in (a) were marked as square and circle dots, respectively. The reduction time of rGO in (a) was 400s.

on the silver surface, the adsorption of RhB is enhanced by the strong π - π interaction between rGO and RhB molecule. The broad peaks at 1336 cm^{-1} and 1594 cm^{-1} are related to the characteristic D peak and G peak of rGO (marked with square and circle dots, respectively). The intensities of Raman characteristic peaks of RhB at 1649 cm^{-1} (aromatic C-C stretching) and 1360 cm^{-1} (aromatic C-C stretching) show a slight increase compared to those obtained at the original silver dendrites due to the double effect of electromagnetic enhancement and chemical enhancement from plasmonic silver and rGO [32]. This means that the wrinkled rGO layer improves the contact with the underlying silver dendrites, allowing an increase in SERS activity [33]. However, the intensity of Raman characteristic peak of RhB at 622 cm^{-1} (aromatic bending) slightly declines, suggesting different enhancement abilities of rGO for different vibrational modes [18]. Compared with the silver dendrites alone, the rGO/Ag nanostructure with the silver NPs dispersed on the rGO surface enhances the Raman signal related to the RhB by about 3 times at the 1649 cm^{-1} band. It indicates that the high-density "hot spots" generated in the nanoscaled junctions and interstices of densely-packed silver NPs (Fig. 1c) can provide a stronger Raman signal. Furthermore, the addition of gold NPs makes the Ag/rGO/Au nanostructure have a remarkable advantage in the enlargement of Raman signal of RhB at 1649 cm^{-1} (8.8-fold increase) compared to the silver dendrites alone. There could be two reasons for the additional enhancement when considering the Ag/rGO/Au hybrid. First, two metal-rGO interfaces in the Ag/rGO/Au sandwich structure could arouse surface plasmons, and the electron accumulation layer formed at both sides of rGO plane due to different dipoles might lead to stronger interface interactions

[34,35]. The rGO interface could effectively transfer excited surface plasmons from silver with large work function to the top gold with small work function [16], resulting in further localized conduction electrons and broadened plasmon resonance on the gold surface [15,16]. Second, recent research demonstrated that the dark plasmon mode could be excited by the vertically incident light in the vertically plasmonic metal sandwich configuration [36,37], which might provide higher local electric field strength and longer electric lifetime for further SERS enhancement. Furthermore, the reduction degree of rGO sheets affects the performance of Ag/rGO/Au hybrid by controlling the plasmonic gold on the rGO surfaces. The enhancement of Raman intensity of RhB adsorbed on Ag/rGO/Au with 800s-reduced rGO (Fig. 4b) can be attributed to more "hot spots" formed among closer large-size gold NPs on rGO surface because the plasmon energy will be raised with size increase of gold particle within the scope of 60 nm [38]. The standard deviation of SERS intensity at 1649 cm^{-1} obtained from six different points is estimated to be $\sim 6.5\%$, indicating the good stability and reproducibility of Ag/rGO/Au hybrid.

We further investigate the SERS sensitivity and antioxidant capacity of Ag/rGO/Au hybrids. Fig. 5(a) shows the SERS spectra of RhB with changeable concentrations on the Ag/rGO/Au structure with the 800s-reduced rGO sheets. The Raman intensity of RhB is weakened with the decreasing concentration of RhB. The Raman response of different vibrational modes exhibits a linear dependence on the RhB concentration from 10 nM to 1000 nM ($R^2 = 0.995$) (Fig. 5b). When the Ag/rGO/Au specimen is further exposed to ambient condition for 0, 10, 50 and 120 days, respectively, the relative Raman intensities of RhB obtained from the average value of

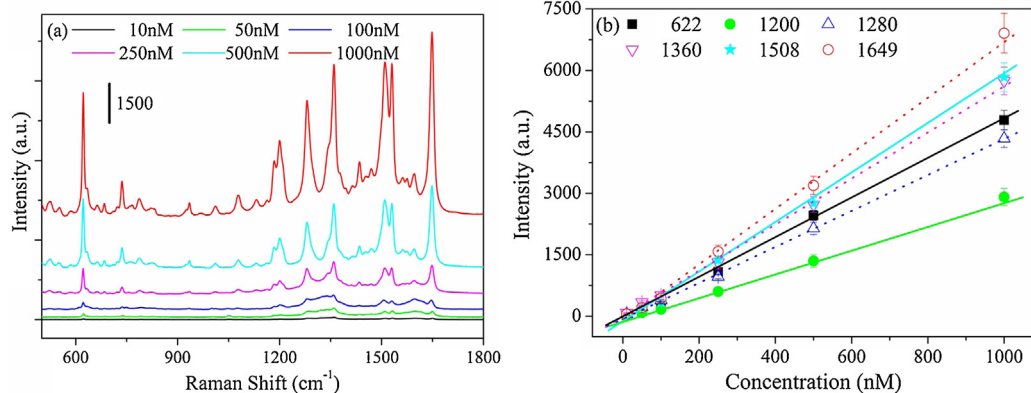


Fig. 5. (a) SERS spectra of different concentrations of RhB adsorbed on Ag/rGO/Au hybrid with the reduction time of rGO for 800s. (b) Linear relation of RhB concentration on peak intensity of Raman signal at different vibrational modes.

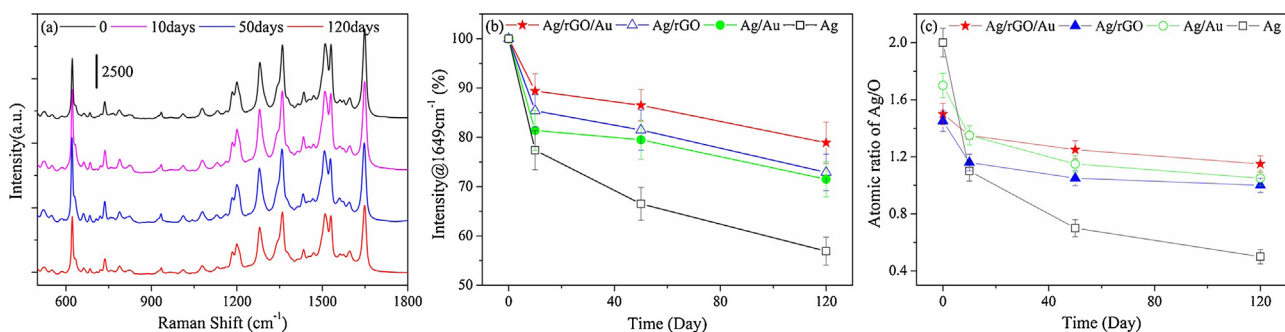


Fig. 6. (a) SERS spectra of 10^{-6} M RhB adsorbed on the Ag/rGO/Au hybrid after exposure to ambient condition for 0, 10, 50 and 120 days, respectively. Dependences of (b) Raman intensity percentage at 1649 cm^{-1} and (c) atomic ratio of Ag/O on exposure time. The reduction time of rGO sheets was 800s.

six-point measurements after 50-day and 120-day exposure decrease by about 10.6% and 13.5% (Fig. 6a-b), respectively, indicating that the rGO interlayer and gold NPs film could protect silver dendrites from oxidation to maintain the SERS activity of Ag/rGO/Au hybrids compared to the plain silver dendrites and Ag/Au hybrids. The XPS results reveal the change of oxygen content in different hybrids over time after exposed to ambient condition. The Ag/O ratio displays a significant decrease with time lengthening for the silver dendrites, implying the aggravated oxidation of silver surface (Fig. 6c). The existence of rGO layer decreases the initial Ag/O ratios at Ag/rGO and Ag/rGO/Au hybrids due to the oxygen-containing groups at rGO surfaces. The slight decrease in the Ag/O ratios over time at Ag/rGO and Ag/rGO/Au hybrids confirm the effective protection of rGO and gold NPs film to silver dendrites from oxidation, as previous reports [11,12].

4. Conclusions

We developed an efficient SERS-based chemical sensor by sandwiching reduced graphene oxide (rGO) sheets between plasmonic silver dendrites and gold nanoparticles layers by a convenient, environmentally friendly and low-cost electrochemical method. The high SERS sensitivity was generated by the combined effect of chemical enhancement of large surface-area rGO with strong absorbed ability to target molecules and the electromagnetic enhancement of plasmonic silver and gold upon illumination. The enhanced interlayer interaction favored the excited surface plasmons transferring from the silver surface to the top gold, resulting in Raman signal enlargement. The SERS signals of Rhodamine B (RhB) molecules absorbed on the Ag/rGO/Au sandwich structure were also tuned by changing the reduction time of rGO which determined the amount of oxygen-containing groups and active site for gold nucleation on rGO surface. The optimal Ag/rGO/Au hybrid presented an 8.8-fold increase in SERS signal of RhB compared to the pristine silver dendrites and showed a low detection limit about 10 nM. Furthermore, the rGO interlayer and gold nanoparticles film protected silver dendrites from oxidation under ambient condition effectively. The simple, rapid and sensitive Raman detection strategy using rGO embedded sandwich structure as a Raman amplifier exhibited a great potential for monitoring of food/environmental safety due to the high sensitivity and long-term stability of sandwich structure.

Acknowledgments

This work was supported by the National Natural Science Foundation of China (Nos. 51272237, 11372280 and 61205158), the China Postdoctoral Science Foundation (Nos. 2012M520063, 2013T60587 and Bsh1201016), the 521 Talent Project of Zhejiang

Sci-Tech University, the Scientific Research Foundation for the Returned Overseas Chinese Scholars (State Education Ministry) and the Technology Foundation for Selected Overseas Chinese Scholar of China.

References

- [1] M. Fleischmann, P.J. Hendra, A. McQuillan, J. Chem. Phys. Lett. 26 (1974) 163.
- [2] C. Fang, A.V. Ellis, N.H. Voelcker, Electrochim. Acta 59 (2012) 346.
- [3] G. Braun, S.J. Lee, M. Dante, T.Q. Nguyen, M. Moskovits, N. Reich, J. Am. Chem. Soc. 129 (2007) 6378.
- [4] A.E. Grow, L.L. Wood, J.L. Claycomb, P.A. Thompson, J. Microbiol. Methods 53 (2003) 221.
- [5] T.R. Jensen, M.D. Malinsky, C.L. Haynes, P. Van Duyne Richard, J. Phys. Chem. B 104 (2000) 10549.
- [6] N. Felidj, J. Aubard, G. Levi, J.R. Krenn, A. Hohenau, G. Schider, A. Leitner, F.R. Aussenegg, Appl. Phys. Lett. 82 (2003) 3095.
- [7] Y. Han, R. Lupitskyy, T.M. Chou, C.M. Stafford, H. Du, S. Sukhishvili, Anal. Chem. 83 (2011) 5873.
- [8] F.X. Liu, Z.S. Cao, C.J. Tang, L. Chen, Z.L. Wang, ACS Nano 4 (2010) 2643.
- [9] J.J. Feng, U. Gernert, P. Hildebrandt, I.M. Weidinger, Adv. Func. Mater. 20 (2010) 1954.
- [10] L. Bao, S.M. Mahurin, S. Dai, Anal. Chem. 76 (2004) 4531.
- [11] Y.K. Kim, S.W. Han, D.H. Min, ACS Appl. Mater. Interfaces 4 (2012) 6545.
- [12] A. Gutes, R. Maboudian, C. Carraro, Langmuir 28 (2012) 17846.
- [13] S. Pande, S.K. Ghosh, S. Praharaj, S. Panigrahi, S. Basu, J. Phys. Chem. C 111 (2007) 10806.
- [14] J.J. Feng, U. Gernert, M. Sezer, U. Kuhlmann, D.H. Murgida, C. David, M. Richter, A. Knorr, P. Hildebrandt, I.M. Weidinger, Nano Lett. 9 (2009) 298.
- [15] C. Sun, K.H. Su, J. Valentine, Y.T. Rosa-Bauza, J.A. Ellman, O. Elboudwarej, B. Mukherjee, C.S. Craik, M.A. Shuman, F.F. Chen, X. Zhang, ACS Nano 4 (2010) 978.
- [16] K.H. Kim, Y.K. Baek, H.J. Jeon, M. Srinivasarao, H.T. Jung, Nanotechnology 23 (2012) 315302.
- [17] K.H. Su, S. Durant, J.M. Steele, Y. Xiong, C. Sun, X. Zhang, J. Phys. Chem. B 110 (2006) 3964.
- [18] X. Ling, L.M. Xie, Y. Fang, H. Xu, H.L. Zhang, J. Kong, M.S. Dresselhaus, J. Zhang, Z.F. Liu, Nano Lett. 10 (2010) 553.
- [19] W. Ren, Y.X. Fang, E.K. Wang, ACS Nano 5 (2011) 6425.
- [20] L.L. Zhang, C.L. Jiang, Z.P. Zhang, Nanoscale 5 (2013) 3773.
- [21] A.P. Liu, T. Xu, Q.H. Ren, M. Yuan, W.J. Dong, W.H. Tang, Electrochim. Commun. 25 (2012) 74.
- [22] G. Goncalves, P.A.P. Marques, C.M. Granadeiro, H.I.S. Nogueira, M. Singh, J. Gracio, Chem. Mater. 21 (2009) 4796.
- [23] A.P. Liu, E.J. Liu, G.C. Yang, N.W. Khun, W.G. Ma, Pure Appl. Chem. 82 (2010) 2217.
- [24] W.S. Hummers, R.E. Offeman, J. Am. Chem. Soc. 80 (1958) 1339.
- [25] N.I. Kovtyukhova, P.J. Ollivier, B.R. Martin, T.E. Mallouk, S.A. Chizik, E.V. Buzanova, A.D. Gorchinskii, Chem. Mater. 11 (1999) 771.
- [26] K.Q. Peng, Y.J. Yan, S.P. Gao, J. Zhu, Adv. Funct. Mater. 13 (2003) 127.
- [27] T.A. Witten, L.M. Sander, Phys. Rev. Lett. 47 (1981) 1400.
- [28] W.C. Ye, C.M. Shen, J.F. Tian, C.M. Wang, L.H. Bao, H.J. Gao, Electrochim. Commun. 10 (2008) 625.
- [29] E. Yoo, T. Okata, T. Akita, M. Kohyama, J. Nakamura, I. Honma, Nano Lett. 9 (2009) 2255.
- [30] J.I. Paredes, S. Villar-Rodil, P. Solís-Fernández, A. Martínez-Alonso, J.M.D. Tasco'n, Langmuir 25 (2009) 5957.
- [31] K. Vinodgopal, B. Neppolian, I.V. Lightcap, F. Grieser, M. Ashokkumar, P.V. Kamat, J. Phys. Chem. Lett. 1 (2010) 1987.
- [32] X.J. Liu, L.Y. Cao, W. Song, K.L. Ai, L.H. Lu, ACS Appl. Mater. Interfaces 3 (2011) 2944.

- [33] W.G. Xu, J.Q. Xiao, Y.F. Chen, Y.B. Chen, X. Ling, J. Zhang, *Adv. Mater.* 25 (2013) 928.
- [34] C. Gong, D. Hinojos, W. Wang, N. Nijem, B. Shan, R.M. Wallace, K. Cho, Y.J. Chabal, *ACS Nano* 6 (2012) 5381.
- [35] A.M. Zaniewski, M. Schriver, J.G. Lee, M.F. Crommie, A. Zettl, *Appl. Phys. Lett.* 102 (2013) 023108.
- [36] Y.C. Chang, S.M. Wang, H.C. Chung, C.B. Tseng, S.H. Chang, *ACS Nano* 6 (2012) 3390.
- [37] S.C. Yang, H. Kobori, C.L. He, M.H. Lin, H.Y. Chen, C.C. Li, M. Kanehara, T. Teranishi, S. Gwo, *Nano Lett.* 10 (2010) 632.
- [38] E.J. Zeman, G.C. Schatz, *J. Phys. Chem.* 91 (1987) 634.